FULL ARTICLE

Fiber attenuated total reflection infrared spectroscopy of kidney tissue during live surgery

Valdas Sablinskas[1]* | Rimante Bandzeviciute[1] | Martynas Velicka[1] |
Justinas Ceponkus[1] | Vidita Urboniene[1] | Feliksas Jankevicius[2,3] |
Arvydas Laurinavičius[4] | Darius Dasevičius[4] | Gerald Steiner[5]*

[1]Institute of Chemical Physics, Vilnius University, Vilnius, Lithuania

[2]Faculty of Medicine, Vilnius University, Vilnius, Lithuania

[3]National Cancer Institute, Vilnius, Lithuania

[4]National Center of Pathology, Affiliate of Vilnius University Hospital Santaros Klinikos, Vilnius, Lithuania

[5]Faculty of Medicine Carl Gustav Carus, Clinical Sensing and Monitoring, Dresden University of Technology, Dresden, Germany

*Correspondence
Valdas Sablinskas, Faculty of Medicine, Vilnius University, Santariskiu str. 2, Vilnius, LT-08661, Lithuania.
Email: valdas.sablinskas@ff.vu.lt

Gerald Steiner, Faculty of Medicine Carl Gustav Carus, Clinical Sensing and Monitoring, Dresden University of Technology, Dresden, Germany.
Email: gerald.steiner@tu-dresden.de

Funding information
Research Council of Lithuania, Grant/Award Number: SEN-16/2015

Abstract

More than 90% of solid kidney tumors are cancerous and have to be treated by surgical resection where surgical outcomes and patient prognosis are dependent on the tumor discrimination. The development of alternative approaches based on a new generation of fiber attenuated total reflection (ATR) probes could aid tumor identification even under intrasurgical conditions. Herein, fiber ATR IR spectroscopy is employed to distinguish normal and cancerous kidney tissues. Freshly resected tissue samples from 34 patients are investigated under nearly native conditions. Spectral marker bands that allow a reliable discrimination between tumor and normal tissue are identified by a supervised classification algorithm. The absorbance values of the bands at 1025, 1155 and 1240 cm^{-1} assigned to glycogen and fructose 1,6-bisphosphatase are used as the clearest markers for the tissue discrimination. Absorbance threshold values for tumor and normal tissue are determined by discriminant analysis. This new approach allows the surgeon to make a clinical diagnosis.
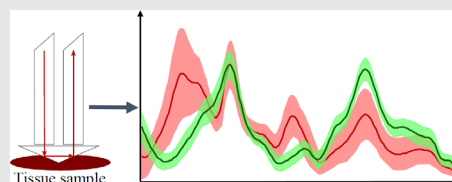
KEYWORDS

ATR, fiber probe, FTIR, kidney cancer, resected tissue

1 | INTRODUCTION

During the past decades, many efforts were made to characterize and to distinguish tissue by vibrational spectroscopy. Although a huge number of successful reports were published dealing with this topic [1–3], the transfer into clinic appears to be limited due to the lack of instruments and systems that allow in situ measurements. While usually Raman spectroscopy is considered as method of

choice for an in situ characterization of tissue [4], infrared (IR) spectroscopy is often seen as laboratory testing method. However, Raman spectroscopy requires often few minutes measurement time to record qualitative spectra and, more important, the question of photo toxicity or photo damaging of the excitation laser is not answered yet. Reasons why IR spectroscopy did not found broad application for in situ diagnosis might be among other things. The strong absorption bands of

water and the fact that IR light is difficult to "transport" to the point of measurements. However, recent developments in IR fiber spectroscopy allow now quick and reliable spectroscopic measurements even of native tissue and opens the door for in situ applications in the clinic. This is mainly driven by the fact that there is big need for surgeons to determine malignancy of tissue during the surgical operation in order to make final decision about exact place of the surgical cut. On the other hand, the evaluation of spectra in regard to classify tissue as normal or pathological is still a challenge.

IR absorption spectra of biological tissue are rather complex and difficult to analyze; nevertheless, during the last decades, there are many successful attempts to apply IR spectroscopy for detection of tumorous tissue areas [5–8], for elucidating structure of kidney, bladder or gall stones [9–12], for analysis of sediments in various bodily fluids [13–15]. Main drawback of this method is that sample for the studies has to be transferred from the patient to the instrument. Using IR fibers in combination with an attenuated total reflection (ATR) crystal may overcome the time consuming ex vivo measurements. However, main drawback of the ATR-FTIR method as a tool for detection of tumorous tissue areas was a lack of suitable fiber probes which provide quick and reliable measurements of native tissue. Two types of fiber ATR probes could be used: ATR crystal probe and loop probe. Generally, both types of probe could be used for tissue examination, but an application of fiber probes for tissue measurements is restricted by the requirement to sterilize them after each use to avoid the contamination of the tissue. This requirement restricts the design of the probes to be easily changeable and sterilizable. Therefore, the tip with ATR crystal is more appropriate for the tissue examination. For this reason, this type of tips was used in designing our fiber ATR FTIR system.

In order to use IR spectroscopy in operating room (OR) there are some requirements concerning size of the instrument and ability to do measurements in situ. There is some choice of portable IR spectrometers in the market, but they are not suitable for the in situ ATR measurement, since they are equipped with compact detector (usually DTGS) which has limited sensitivity. Such in situ measurements require a fiber probe with ATR tip attached to the end of the fiber. Usually, in such fiber arrangement loses of optical signal are 90% or even larger, what makes the measurements meaningless.

In an early study, we have demonstrated that very small areas of infiltrated kidney tumor can be detected by IR spectroscopic imaging and supervised classification [16]. In the next study, we found a particular spectral region that contains spectroscopic signals from extracellular and intracellular molecules such as fatty acids, glycerol and glycogen. The signals can be used as spectral markers for classification of healthy and tumor cells of kidney tissue [17]. These initial studies were focused mainly on determining whether and where reliable spectral differences between normal and tumor kidney tissue are located.

Also, we have demonstrated that kidney tumor tissue can be identified by measuring spectra of dried tissue smears by using a portable IR spectrometer equipped with a new type of a fiber ATR probe [18]. In the present study, we demonstrate that kidney tumor tissue can be identified during live surgery using this fiber setup for the measurements of wet tissue nearly in its native conditions. In contrast to other studies, the spectra are not classified and results are not translated into a computer based diagnose like "tumor" or "healthy." Aimed on the clinical application and in accordance to the regulations in medicine, the concrete absorbance values of the marker spectral bands are defined and represented without any algorithm-based classification.

2 | EXPERIMENTAL

Spectra of tissue were measured using ATR silver halide fiber probe attached to the standard FTIR spectrometer Alpha (Bruker Optik GmbH, Ettlingen, Germany). Changeable fiber probe tips with single reflection germanium ATR crystal were used. The schematics of the ATR fiber probe (Art Photonics GmbH, Berlin, Germany) accessory is presented in Figure 1.

The development of the complete system was implemented by our researchers' group in cooperation with "Art Photonics." Optical fibers used in the setup are made from silver halide. The focusing and directing of the light in this accessory is done only by two elliptical and four flat mirrors. The germanium ATR crystal is fixed to the fiber by means of detachable plastic holder (tip). Such approach gives an opportunity for a new and sterile tip to be used for every successive measurement and ensures that no contaminants are introduced to the tissue thus reducing the risk of the complications during
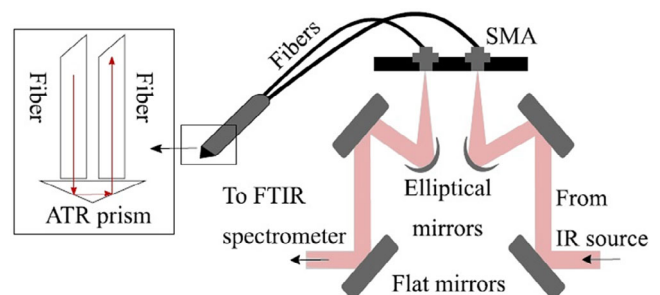

FIGURE 1 Schematic diagram of fiber attenuated total reflection (ATR) probe with changeable ATR crystal

the surgery. The ATR fiber accessory is made in a compact way and allows the quick interchanging from the conventional ATR setup of the portable FTIR spectrometer and the ATR fiber setup without the need to use two different spectrometers.

A liquid nitrogen cooled MCT detector (Infrared Associates, Inc. Model IRA-20-00131) was coupled with the whole system in order to compensate the loss of optical signal in the fiber which leads to the reduction of signal-to-noise ratio. This spectroscopy system is rather light and compact thus it can be easily fitted on a mobile table for maneuverability.

The main advantage of the application of fiber probes is that the sample could be analyzed in situ conditions and it does not have to be transferred to the device. Also, there are some drawbacks of the fiber ATR setup. The spectral region is restricted due to scattering of light in the fiber but it does not have impact while analyzing the fingerprint spectral region. While performing measurements in fiber ATR configuration the loss of optical signal is current; however, it could be compensated by using more sensitive MCT detector. Fibers made of silver halide are fragile and degradation of the fiber could be observed.

The IR absorption spectra of freshly resected human kidney tissues, taken from 34 patients, were measured immediately after surgical resection inside the operation theater of the Vilnius university hospital Santaros Clinics urology department. The protocol for spectroscopic studies was approved by Vilnius regional bioethics committee (approval No. 158200-15-803-312). Before each measurement, a background spectrum was recorded from the clean ATR fiber probe. Small amounts of suspected tumorous and normal (border tissue around the tumor expected to be normal) tissue were examined. The ATR probe was gently pressed to the freshly cut area of resected kidney tissue sample and spectra of the tissue were collected. IR absorption spectra of tumorous and normal human kidney tissue were measured in 400 to 4000 cm^{-1} spectral region with 4 cm^{-1} spectral resolution. Sixty-four interferograms were averaged and Fourier transformed into a spectrum applying three-term Blackman-Harris apodization function and zero filling factor of 2.

Evaluation of spectral data was performed using the MATLAB Package (Version 7, Math Works Inc. Natick, Massachusetts). In order to minimize the data volume and to exclude the strong absorption bands of water only the region between 950 and 1350 cm^{-1} was considered. Data preprocessing involved a linear baseline correction by using the msbackadj function of the Statistics Toolbox of MATLAB. The baseline correction was performed to reduce influences of light scattering. Spectra with a maximum absorbance larger than 1.8 or smaller than 0.02 were identified as outliers and removed from the data set. Finally, the selected spectra were area-normalized to eradicate spectral

differences due to different sampling conditions during the measurements of different samples. Different overall absorption values of different samples are influenced by several factors. One of the main factors is the contact between the sample and the ATR crystal; in different measurements, it is impossible to ensure the same pressing force on the sample. The consistency and hardness of the samples are also different, especially between normal and tumorous tissues due to different amount of water and biochemical composition. A training set of 24 spectra of each class was built for supervised classification. Aim of the supervised classification was used to explore optimal spectral regions for discrimination of normal and tumor tissue. The approach uses a genetic algorithm to maximize the classification rate with the iterative optimization of selected features and is similar to a method described elsewhere [19]. Each spectrum was reexpressed as a set of three intensity values, which were used for the subsequent classification by quadratic discriminant analysis, done using the classify function available in the Statistics Toolbox of MATLAB. The performance of the classification was assessed with the leave-one-out-validation method. An independent test set of 10 patients was used to test the discrimination parameters.

3 | RESULTS AND DISCUSSION

Examples of resected kidney tissue are represented in Figure 2. While general differences between normal
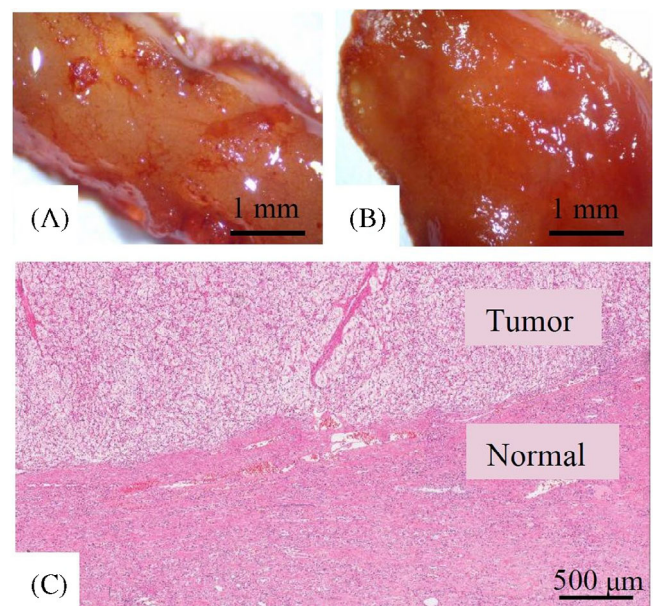

FIGURE 2 Photographs of normal, A, and tumorous, B, tissue samples, microscopy image of H&E stained tissue, C. After microscopic histopathological examination, the borderline between normal and tumorous kidney tissues is clearly visible

TABLE 1 Diagnosed types of kidney tumors

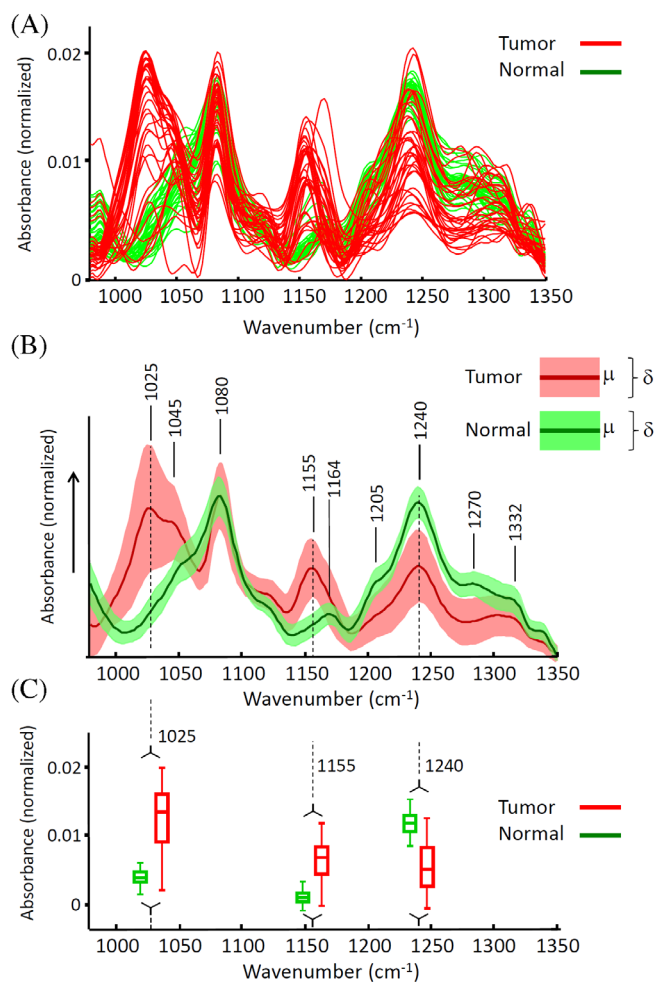| Diagnosis	Number of cases
Clear cell renal cell carcinoma	22
Clear cell renal cell carcinoma, retention cysts	4
Papillary renal cell carcinoma	1
Papillary urothelial carcinoma	1
Chromophobe renal cell carcinoma	3
Chromophobe renal cell carcinoma, retention cysts	1
Oncocytoma, retention cysts	1
SDHB renal cell carcinoma	1

Abbreviation: SDHB, succinate dehydrogenase deficient.

FIGURE 3 A, Spectra of normal (green) and tumor tissue (red). Spectra were preprocessed as described and area normalized. B, Plot of the mean (μ) spectra (bold) and standard deviation (δ) bands. Differences between the spectral profiles of tumor and normal tissue become clearly visible. C, Box whisker plot of selected spectral regions. The three spectral regions were identified as best positions by a supervised classification algorithm as described elsewhere [27]

(Figure 2A) and tumor tissue (Figure 2B) were in the most cases visible, a sharp borderline is not observable. The borderline becomes clearly visible after microscopic histopathological examination (Figure 2C).

For each case, one part of the resected tissue was examined by standard histopathological analysis; another part of sample was used for the measurements of IR absorption spectra. Diagnosed types of kidney tumors and number of cases are summarized in Table 1.

Figure 3A shows the recorded raw ATR spectra of all tumor (red) and normal (green) tissue samples. Due to the strong water absorption bands, spectra were reduced to the spectral region from 950 to 1350 cm^{-1}. At the first glance, the most important spectral bands that may allow to discriminate tumor from normal tissue are located around 1025 and 1155 cm^{-1}.

Between 1000 and 1250 cm^{-1} absorption bands mainly due to carbohydrates, glycoproteins and phosphate groups occur. Clearly, the IR spectrum captures a wealth of chemical information and slight variations in the band positions and intensities reveal heterogeneity across the samples. The key question addressed here is whether the biochemical information latent in these spectra is able to discriminate normal from tumor tissue. The absorption profile between 1000 and 1050 cm^{-1}, in particular the absorption band around 1025 cm^{-1} is stronger for tumor tissue than for normal tissue. Furthermore, tumor tissue exhibits also stronger absorption around 1150 cm^{-1} and weaker signals between 1200 and 1275 cm^{-1}. The question that then arises is which constituents could be responsible for these bands. To illustrate the spectral changes more clearly, Figure 3B shows the average spectra and standard deviation of both types of the tissue. Table 2 summarizes the vibrational modes in this spectral range.

The spectral band at 1025 cm^{-1} is assigned to $\nu(C\!-\!O)$, $\nu(C\!-\!C)$ stretching and $\delta(C\!-\!O)$ bending

vibrations of C—OH groups of glycogen while the band at 1155 cm^{-1} is attributed to the $\nu(C\!-\!O)$ stretching vibrations [24]. Spectra of tumor tissue clearly show a higher intensity at 1025 and 1155 cm^{-1}. It is known that kidney tumor cells tend to store glycogen in their cytosol [25]. Generally, the stronger absorption signals arise because tumor cells have a higher demand of energy than normal cells because of their fast proliferation.

In case of clear cell renal cell carcinoma tumors, the amount of fructose 1,6-bisphosphatase is decreased [25, 26]. Tumor cells express less of fructose 1,6-bisphosphatase thus reinforces Warburg-like metabolic shift. Decreased amount of this enzyme is associated with changed cellular metabolic processes and increased amount of glycolytic flux in tumorous cells as fructose 1,6-bisphosphatase antagonizes

TABLE 2 IR absorption spectral bands of kidney tissue in the spectral region from 950 to 1350 cm^{-1} and their assignments [20–23]

Spectral position (cm^{-1})	Assignment
1025	ν(C—O), ν(C—C), δ(C—O)
1045	ν(C—O), δ(C—OH)
1080	ν_s(PO$_2^-$)
1155	ν(C—O)
1164	ν(C—C), ν(C—O), δ(C—OH)
1205	ν(C—O—C), ν(C—O), amide III
1240	ν_{as}(PO$_2^-$)
1270	CH$_2$ rocking
1332	CH$_2$ wagging

Abbreviation: IR, infrared.

TABLE 3 Defined thresholds of absorbance values (A) to discriminate tumor from normal tissue

Spectral position (cm^{-1})	Tumor	Normal
1025	$A \geq 0.0064$	$A < 0.0064$
1155	$A \geq 0.005$	$A < 0.005$
1240	$A \leq 0.01$	$A < 0.01$

the glycolytic flux and inhibits the nuclear function of HIF-α metabolic regulator [25, 26]. The band located at 1240 cm^{-1} is assigned to $\nu(\text{PO}_2^-)$ asymmetric stretching vibrations and to the amide III mode of proteins [24]. Hereby, the decreased absorbance value of this band possibly could be related with lower concentration of fructose 1,6-bisphosphatase.

The optimization classification procedure of the algorithm selects the best number of spectral bands and their spectral positions. In respect to a practical use, in particular that the surgeon has to define the diagnosis based on the intensity of spectral marker bands, the maximum number of selected bands used for the genetic algorithm was set to five. An optimized classification result could be obtained by three selected bands. When the algorithm involves more than three bands the accuracy of the trainings set becomes not better and the risk of an over determination increases. Therefore, a leave-one-out validation was used to avoid an over-determination by too many classifiers. It has to be noted that all three bands are necessary for a successful classification and all bands have the same "importance" for the classification result or diagnosis, respectively. The optimal separation between normal and tumor tissue was determined by linear discriminant analysis. Thresholds of absorbance values (A) are listed in Table 3. It has to be noted that the defined thresholds are referred to area normalized spectra as described above.

The absorbance values were determined and plotted in Figure 4. After tissue discrimination according to the defined thresholds, all normal tissue samples were identified correctly. Then, 27 of 34 kidney tumor samples were correctly classified as tumor tissues. In two cases (#8 and #33) tumor tissue and partly normal tissue exhibit absorbance values of the other, wrong tissue class. These two cases are diagnosed as papillary renal cell carcinoma and succinate dehydrogenase-deficient renal cell carcinoma with retention cysts. Only single cases of papillary renal cell carcinoma and succinate dehydrogenase-deficient renal cell carcinoma with retention cysts were observed during the study, while the most frequent type of kidney tumors is clear cell renal cell carcinoma. Due to specific biochemical processes in different tumor types, different spectral markers are required for discrimination of various tumor types.

In three cases (patients #7, #27 and #29), tumorous tissue samples were classified as questionable. In these cases, patients were diagnosed with chromophobe renal cell carcinoma (patient #29), chromophobe renal cell carcinoma with retention cysts (patient #27) and clear cell renal cell carcinoma with retention cysts (patient #7). Specific morphological features of chromophobe renal cell carcinoma may produce specific IR spectra that discriminate this tumor type from other kidney tumors. During the study 50% (patient #17 and #22) of chromophobe renal cell carcinoma samples were identified as tumorous tissue and 50% (patients #29 and #27) as questionable tissue. It could be linked to the fact that chromophobe renal cell carcinoma morphologically has "classic" and eosinophilic types. The latter has significant overlap with oncocytoma and often poses a diagnostic problem. The basic chromophobe cell type is characterized by large polygonal cells with a transparent, slightly reticulated cytoplasm with prominent cell membranes leading to a plant cell-like appearance. Electron microscopically, the cytoplasm is crowded by loose glycogen deposits and numerous, sometimes invaginated and studded vesicles. The second cell type in chromophobe renal cell carcinoma is also characterized by an increased cytoplasmic eosinophilia or granularity, due to an augmentation of mitochondria. Both cell types can occur singly or in combination within a given tumor. On the assumption that in one part of chromophobe renal cell carcinoma tumors, the amount of glycogen is altered, those tissues could be classified as tumorous tissue as in case of clear cell renal cell carcinoma which has specific biochemical feature of increased amount of lipids and glycogen. In case when loose glycogen is not apparent in the cells, it leads to the misclassification of tissue. Chromophobe renal cell carcinoma is infrequently occurring type of kidney tumors
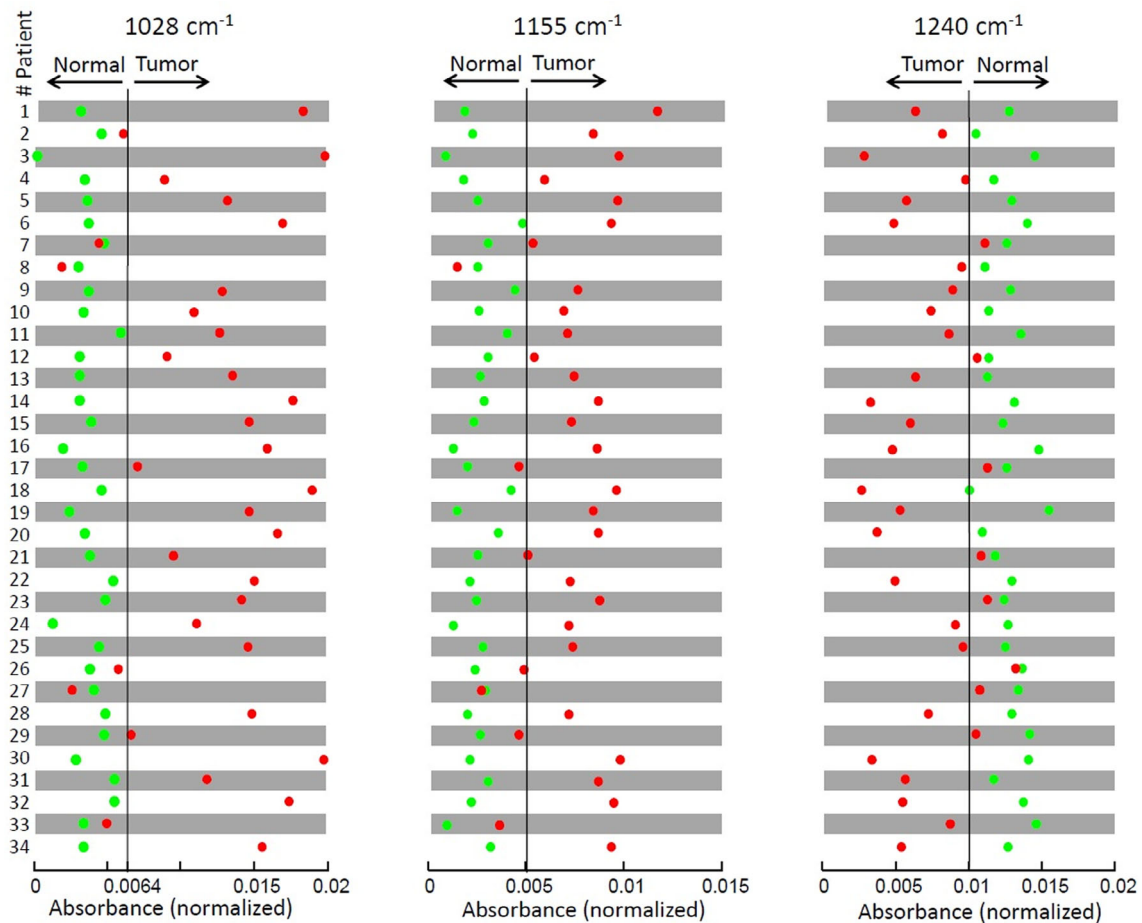
FIGURE 4   Representing spectroscopic diagnostic information similar to the standard form of laboratory-analyzed findings. The figure shows a plot of the absorbance values at the selected spectral regions of normal (green) and tumor (red) tissue. Spectra of patients #1 to #24 were used as training set for determination of optimal spectral regions. Ten Spectra (#25 to #34) were classified as independent test set. In this figure, the spectral data of patients #1 to #24 are reclassified

and different spectral markers are required for tissue discrimination. For the more detailed conclusions, more cases of chromophobe renal cell carcinoma should be investigated.

In two cases (patients #2 and #26), tissue samples were identified as suspected to be tumorous. In these cases, patients were diagnosed with clear cell renal cell carcinoma with retention cysts. In most cases, when the retention cysts are present, tissues are not classified as tumorous. The presence of retention cysts disables to recognize the tissue type according to changed concentrations of biochemical components that could be assigned as markers of cancer.

The results indicate that fiber ATR IR spectroscopy could be used to aid clinical differentiation of normal and tumor kidney tissue in a fast and sensitive way during live surgery. It should be noted that the presentation of spectral markers values in the form of laboratory data, without computer-based classification, enables a real clinical application of the spectroscopic approach. The final goal of such spectroscopic approach is to detect the hard-to-see borderlines under intraoperative conditions, because an incomplete removal of the tumor is linked to recurrences which dramatically reduce the prognosis of the patient. This is the preclinical trial, so validation by a larger sample set is the next step followed by an adaption of the fiber optic probe for in situ applications.

The initial results of this study are promising and demonstrate that the core idea is rather round.

4 | CONCLUSION

In conclusion, this work has shown that fiber ATR IR spectroscopy is suitable to obtain meaningful spectra of normal and tumorous kidney tissues. The spectra of both types of tissue contain enough information for the tissue discrimination. Spectral bands at 1025 and 1155 cm^{-1} assigned to glycogen and the band at 1240 cm^{-1} assigned to fructose 1,6-bisphosphatase were considered as spectral markers for tumorous tissue identification. In case of

tumorous tissue of the intensity of the spectral bands, corresponding to glycogen gets higher, while the absorbance of the band corresponding to fructose 1,6-bisphosphatase gets lower. Concrete intensity values of marker spectral bands used for the discrimination of normal and tumorous tissue were defined. Identification of tumorous tissue in case of presence of retention cysts in it can leads to misclassification due to changed concentrations of biochemical components that are present in cancerous tissue. The newly designed fiber probe could be developed in the future; method has potential to be moved towards intrasurgical applications for the more efficient surgical treatment.

ACKNOWLEDGMENT

CONFLICT OF INTEREST

The authors declare no financial or commercial conflict of interest.

AUTHOR CONTRIBUTIONS

F. J., A. L. and D. D. were involved in sample preparation and histopathological analysis, V. S. was involved in conceptualization and project management, G. S. was involved in conceptualization, statistical analysis, writing and editing, R. B. was involved in investigation and writing and J. C., M. V. and V. U. were involved in the experiment setup.

DATA AVAILABILITY STATEMENT

Data can be requested from the authors.

ORCID

Gerald Steiner https://orcid.org/0000-0002-7625-343X

REFERENCES

[1] R. K. Sahu, S. Mordechai, *Future Oncol.* **2005**, *1*, 635.
[2] D. P. Lau, Z. Huang, H. Lui, C. S. Man, K. Berean, M. D. Morrison, H. Zeng, *Lasers Surg. Med.* **2003**, *32*, 210.
[3] F. M. Lyng, D. Traynor, T. N. Q. Nguyen, A. D. Meade, F. Rakib, R. Al-Saady, E. Goormaghtigh, K. Al-Saad, M. H. Ali, *PLoS One* **2019**, *14*, e0212376.
[4] C. Krafft, J. Popp, *J. Anal. Bioanal. Chem.* **2015**, *407*, 699.
[5] G. Bellisola, C. Sorio, *Am. J. Cancer Res.* **2012**, *2*, 1.
[6] S. E. Taylor, K. T. Cheung, I. I. Patel, J. Trevisan, H. F. Stringfellow, K. M. Ashton, N. J. Wood, P. J. Keating, P. L. Martin-Hirsch, F. L. Martin, *Br. J. Cancer* **2011**, *104*, 790.
[7] X. Sun, Y. Xu, J. Wu, Y. Zhang, K. Sun, *J. Surg. Res.* **2013**, *179*, 33.
[8] S. Kumar, A. Srinivasan, F. Nikolajeff, *Curr. Med. Chem.* **2018**, *25*, 1055.
[9] S. Tamosaityte, V. Hendrixson, A. Zelvys, R. Tyla, Z. A. Kucinskiene, F. Jankevicius, M. Pucetaite, V. Jablonskiene, V. Sablinskas, *J. Biomed. Opt.* **2013**, *18*, 027011.
[10] M. Pucetaite, S. Tamosaityte, A. Engdahl, J. Ceponkus, V. Sablinskas, P. Uvdal, *Cent. Eur. J. Chem.* **2014**, *12*, 44.
[11] O. Kleiner, J. Ramesh, M. Huleihel, B. Cohen, K. Kantarovich, C. Levi, B. Polyak, R. S. Marks, J. Mordehai, Z. Cohen, S. Mordechai, *BMC Gastroenterol.* **2002**, *2*, 2. https://doi.org/10.1186/1471-230X-2-3.
[12] C. B. J. Ha, S. Park, *Biomater. Res.* **2018**, *22*, 22. https://doi.org/10.1186/s40824-018-0128-8.
[13] J. R. Hands, G. Clemens, R. Stables, K. Ashton, A. Brodbelt, C. Davis, T. P. Dawson, M. D. Jenkinson, R. W. Lea, C. Walker, M. J. Baker, *J. Neurooncol* **2016**, *127*, 463.
[14] A. Takamura, K. Watanabe, T. Akutsu, T. Ozawa, *Sci. Rep.* **2018**, *8*, 8459.
[15] K. V. Oliver, A. Vilasi, A. Maréchal, S. H. Moochhala, R. J. Unwin, P. R. Rich, *Sci. Rep.* **2016**, *6*, 34737.
[16] V. Sablinskas, V. Urboniene, J. Ceponkus, A. Laurinavicius, D. Dasevicius, F. Jankevicius, V. Hendrixson, E. Koch, G. Steiner, *J. Biomed. Opt.* **2011**, *16*, 096006.
[17] V. Urboniene, M. Pucetaite, F. Jankevicius, A. Zelvys, V. Sablinskas, G. Steiner, *J. Biomed. Opt.* **2014**, *19*, 087005.
[18] V. Sablinskas, M. Velicka, M. Pucetaite, V. Urboniene, J. Ceponkus, R. Bandzeviciute, F. Jankevicius, T. Sakharova, O. Bibikova, G. Steiner, *Proc. SPIE* **2018**, *10497*, 1049713.
[19] A. E. Nikulin, B. Dolenko, T. Bezabeh, R. L. Somorjai, *NMR Biomed.* **1998**, *11*, 209.
[20] G. I. Dovbeshko, N. Y. Gridina, E. B. Kruglova, O. P. Pashchuk, *Talanta* **2000**, *53*, 1, 233.
[21] G. Socrates, *Infrared and Raman Characteristic Group Frequencies*, Wiley, West Sussex **2001**.
[22] G. I. Dovbeshko, V. I. Chegel, N. Y. Gridina, O. P. Repnytska, Y. M. Shirshov, V. P. Tryndiak, I. M. Todor, G. I. Solyanik, *Biopolymers* **2002**, *67*, 470.
[23] M. Jackson, H. H. Mantsch, *Pathology by Infrared and Raman Spectroscopy, Handbook of Vibrational Spectroscopy*, John Wiley & Sons, Hoboken, New Jersey, **2006**.
[24] Z. Movasaghi, S. Rehman, I. U. Rehman, *Appl. Spectrosc. Rev.* **2008**, *43*, 134.
[25] I. J. Frew, H. Moch, *Annu. Rev. Pathol.* **2015**, *10*, 263.
[26] Y. Xiao, D. Meierhofer, *Int. J. Mol. Sci.* **2019**, *20*, 3672.
[27] G. Steiner, S. Küchler, A. Hermann, E. Koch, R. Salzer, G. Schackert, M. Kirsch, *Cytometry A* **2008**, *73A*, 1158.

SUPPORTING INFORMATION

Additional supporting information may be found online in the Supporting Information section at the end of this article.